


Article

Structural Performance of Cold-Formed Steel Face-to-Face Built-Up Channel Sections under Axial Compression at High Temperatures through Finite Element Modelling

Yecheng Dai ¹ , Krishanu Roy ^{2,*}, Zhiyuan Fang ^{1,2}, Gary M. Raftery ¹ and James B. P. Lim ^{1,2}

¹ Department of Civil and Environmental Engineering, The University of Auckland, Auckland 1023, New Zealand

² School of Engineering, The University of Waikato, Hamilton 3216, New Zealand

* Correspondence: kris.roy@waikato.ac.nz

Abstract: This paper studies the structural performance of cold-formed steel (CFS) face-to-face (FTF) built-up channel sections subjected to axial compression at high temperatures. The material properties of G250 and G450 CFS channel sections at room and high temperatures were acquired from the literature, and the range of temperatures was from 20 to 700 °C. The influences of the section thickness, member length, screw number, and high temperature on the structural performance of such channel sections were examined via a comprehensive parametric analysis involving 576 validated finite element models. As the temperature increased from 20 to 700 °C, the mean axial capacity of the CFS-FTF built-up unlippped and lippped channel sections decreased by 88.9% and 90.2%, respectively. Based on the results of the parametric study, new design equations for the axial capacity of CFS-FTF built-up channel sections at high temperatures were proposed. The mean ratio of the EWM strengths calculated using the American standard (AISI 2016) and Australian/New Zealand standard (AS/NZS 2018) to the FE strengths was 0.77, while the mean ratio of the proposed design strengths to the FE strengths was 1.01. Finally, a reliability analysis was conducted, and it was found that the proposed equations could come close in predicting the axial capacity of CFS-FTF built-up channel sections at high temperatures.

Keywords: cold-formed steel; built-up section; high temperature; finite element analysis; design guidelines



Citation: Dai, Y.; Roy, K.; Fang, Z.; Raftery, G.M.; Lim, J.B.P. Structural Performance of Cold-Formed Steel Face-to-Face Built-Up Channel Sections under Axial Compression at High Temperatures through Finite Element Modelling. *Buildings* **2023**, *13*, 305. <https://doi.org/10.3390/buildings13020305>

Academic Editors: Keerthan Poologanathan, Gatheeshgar Perampalam, Shanmuganathan Gunalan and Marco Corradi

Received: 14 December 2022

Revised: 8 January 2023

Accepted: 17 January 2023

Published: 19 January 2023



Copyright: © 2023 by the authors. Licensee MDPI, Basel, Switzerland. This article is an open access article distributed under the terms and conditions of the Creative Commons Attribution (CC BY) license (<https://creativecommons.org/licenses/by/4.0/>).

1. Introduction

The structural engineering applications of cold-formed steel (CFS) are increasing steadily, with the use of face-to-face (FTF) built-up cold-formed steel channel sections becoming popular as compression members. A CFS-FTF built-up channel section is built by assembling single channels on a face-to-face basis utilising fasteners. The structural application of CFS-FTF built-up channel sections comprises columns in portal frames, struts, and wall studs [1,2]. Understanding the structural behaviour of CFS-FTF built-up channel sections at high temperatures is crucial to minimising the harm brought on by fire-associated incidents. This paper aims to study the influence of high temperatures on the compressive performance of CFS-FTF built-up channel sections.

Regarding the studies reported in the literature on the reduced mechanical properties of CFS sections at elevated temperatures, some researchers have focused on the structural behaviour of different CFS sections at elevated temperatures and subjected to different loading conditions. Researchers have so far examined the compressive performance of CFS single columns at high temperatures. Gunalan et al. [3] experimentally and numerically investigated the local buckling performance of CFS unlippped and lippped channel sections at high temperatures. Gunalan et al. [4] also studied the combined flexural and torsional buckling performance of CFS lippped channels under axial compression at high temperatures. The fire code Eurocode 3 Part 1.2 was found to result in overly conservative

predictions for CFS single columns at high temperatures subjected to local buckling [3] and flexural-torsional buckling [4]. Ranawaka and Mahendran [5] carried out an investigation to study the distortional buckling performance of CFS lipped channel sections under axial compression at high temperatures. The results demonstrated the importance of using accurate mechanical properties at elevated temperatures in the fire safety design of CFS compression members. Chen and Young [6] numerically investigated the structural performance of CFS lipped channel sections under axial compression at high temperatures. A full strain range expression up to the ultimate tensile strain for the stress–strain curves of cold-formed carbon steel at high temperatures was proposed. Feng and Wang [7] studied the compressive performance of CFS channels at room temperature and high temperatures. It was observed that the failure modes of two nominally identical columns could be different, even though the failure loads were close. Multiple investigations have been conducted to determine the effect of high temperatures on CFS single beams. Landesmann and Camotim [8] presented an FE investigation on the distortional buckling behaviour of CFS single-span lipped channel beams under high temperatures. The end-support conditions and cross-section dimensions were found to significantly affect the distortional post-buckling response. Laim et al. [9] conducted a study to understand the structural performance of CFS beams in fire. CFS beams can be strongly affected by the stiffness of the surrounding structures. Kankanamge and Mahendran [10] presented a validated FE model for determining the structural behaviour of CFS lipped channel beams under bending at high temperatures. Fang et al. [11] carried out a numerical simulation to investigate the structural behaviour of CFS single beams with web openings subjected to web crippling. The average web crippling strength was found to decrease by 90% when the temperature increased from 20 to 700 °C.

Only limited research has been reported on the mechanical behaviour of CFS built-up columns under fire in the literature. Fang et al. [12] performed a numerical analysis of the structural performance of CFS built-up perforated channel sections that were connected back to back, where the temperature varied from 20 to 700 °C. A decrease was observed in the axial strength of perforated BTB channels of 87% on average [12]. Yang et al. [13,14] conducted an experimental test to explore the fire performance of CFS-FTF gapped built-up channel columns (see Figure 1a). The influences of the temperature distribution pattern and heating rate on the fire response of such columns were reported. The results indicated that the primary failure mode of the specimens was a combination of local and global flexural buckling, which was sensitive to the longitudinally non-uniform temperature field [13,14]. Pires et al. [15] tested 10 specimens of CFS-FTF built-up channel columns (see Figure 1b). A plasterboard hollow encasement was found to be an alternative that could improve the performance of fire resistance for such columns. However, the cross-section shapes of these CFS-FTF built-up channels did not comprise all of the popular cross-sections (e.g., Figure 1c). More importantly, the current design guidelines of the American standard (AISI 2016) [16] and the Australian/New Zealand standard (AS/NZS 2018) [17] could be inaccurate in predicting different built-up cross-sections.

A numerical investigation is performed in this paper to study the structural performance of CFS-FTF built-up channel sections under axial compression at high temperatures. Figure 1d,e display the dimensions of the CFS-FTF built-up channel sections investigated herein. Based on the Finite Element (FE) results of 576 validated models, a parametric analysis was performed to study the influences of the section thickness, member length, screw number and high temperature on the axial capacity of CFS-FTF built-up channel sections. The results calculated in terms of the AISI (2016) [16] and AS/NZS (2018) [17] design standards were compared with the numerical failure loads of CFS-FTF built-up channel sections subjected to axial compression to examine the accuracy of the current design standards [16,17]. Based on the parametric study results, new design equations were proposed for CFS-FTF built-up channel sections subjected to axial compression at high temperatures, and a reliability analysis was carried out to assess the viability of the proposed design equations.

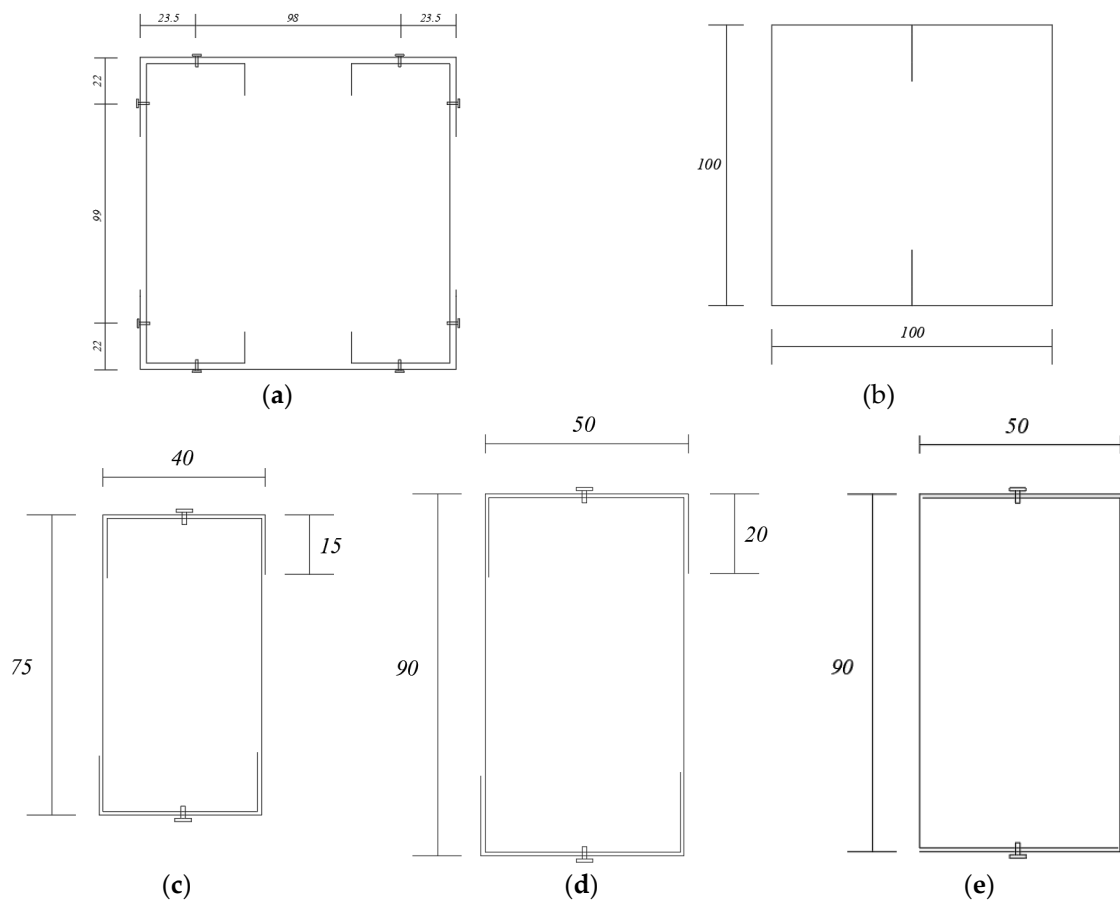


Figure 1. CFS-FTF built-up cross-section shapes: (a) FTF gapped built-up section [13,14]; (b) FTF lip connected built-up section [15]; (c) FTF flange connected built-up section [2]; (d) FTF built-up lipped channel section; and (e) FTF built-up unlipped channel section.

2. Summary of Previous Experiments

Roy et al. [2] and Selvaraj and Madhavan [18] conducted experiments to study the structural performance of CFS-FTF built-up channel sections subjected to axial compression at room temperature. The experiments were carried out at ambient temperature and included different geometric parameters that affect the axial capacity of such sections. These parameters comprised the member length, section dimension, and number of screws. Therefore, the test results presented by Roy et al. [2] and Selvaraj and Madhavan [18] were utilised to validate the FE models.

3. Finite Element Analysis

3.1. General

The ABAQUS [19] was utilised to generate FE models to acquire the axial capacity of CFS-FTF built-up channel sections at high temperatures.

3.2. Material Properties

The stress–strain curves of G250 CFS with 1.55 mm and 1.95 mm thicknesses, as well as G450 CFS with 1.50 mm and 1.90 mm thicknesses, at room and high temperatures were acquired from [20] and applied in the finite element modelling (FEM). Table 1 displays the material properties considered in this study.

Table 1. Material properties of G450 and G250 [20].

Temperature (°C)	G450_1.5 mm		G450_1.9 mm	
	E (MPa)	f_y (MPa)	E	f_y
20	207,490	537.1	206,328	514.5
100	189,375	526.4	196,540	521.2
200	172,000	534.4	173,337	509.9
300	157,380	508.6	148,395	483.6
400	126,030	373.3	118,533	362.2
500	96,800	193.4	77,100	197.1
600	63,126	59.1	52,536	56.6
700	47,559	32.8	24,286	34.0
Temperature (°C)	G250_1.55 mm		G250_1.95 mm	
	E	f_y	E	f_y
20	204,385	293.5	188,220	270.51
100	191,505	279.1	179,640	267.3
200	160,555	274.4	171,745	257
300	142,470	187.8	154,330	196.4
400	128,220	144.4	121,230	147.7
500	81,096	94.8	90,631	95.8
600	62,066	66.3	57,777	54.1
700	24,851	37.3	31,363	34.4

3.3. Specimen Labels

This study utilised CFS-FTF built-up channel sections (unlipped and lipped) with a web depth and flange width of 90 mm and 50 mm, respectively (see Figure 1d). The investigated CFS-FTF built-up channel sections were labelled to express the cross-sectional type, column length, section thickness, and screw numbers. For instance, the interpretations of “BU-L300-t1.5-S2-T20” and “BL-L300-t1.5-S2-T20” are shown below:

- “BU” identifies the unlipped channel section;
- “BL” identifies the lipped channel section;
- “L300” identifies the column length (L) at 300 mm;
- “t1.5” identifies the section thickness (t) at 1.5 mm;
- “S2” indicates that the screw number (S) is 2;
- “T20” identifies the temperature (T) at 20 °C;

It should be noted that the screws were evenly arranged along the column, while the distance from the side screw to the column end was 50 mm.

3.4. Finite Element Mesh

The S4R shell element was used in the FEM of the CFS-FTF built-up channel columns. This element is a thin, shear, flexible, isoparametric and quadrilateral shell with four nodes and five degrees of freedom per node, which utilises reduced integration and bilinear interpolation schemes. Such a shell element can save on computational time since it allows the modelling of thin-walled members with relatively fewer elements than solid elements, and it was applied by past researchers for cold-formed members [21–23]. Both the bottom and top endplates were modelled utilising R3D4 shell elements. This element is a rigid quadrilateral with four nodes and three translational degrees of freedom per node. As the element has no rotational degrees of freedom, the perpendicular shell elements attached by common nodes to a rigid surface comprising R3D4 elements are free to rotate around the attached edge. The local buckling rotations are, therefore, unconstrained. In terms of the mesh sensitivity analysis accounting for the computational efficiency and numerical accuracy, a 10 mm × 10 mm mesh size was applied to the channel section and endplates. A finer mesh size was taken into account near the corners for better accuracy in the FEM, as shown in Figure 2.

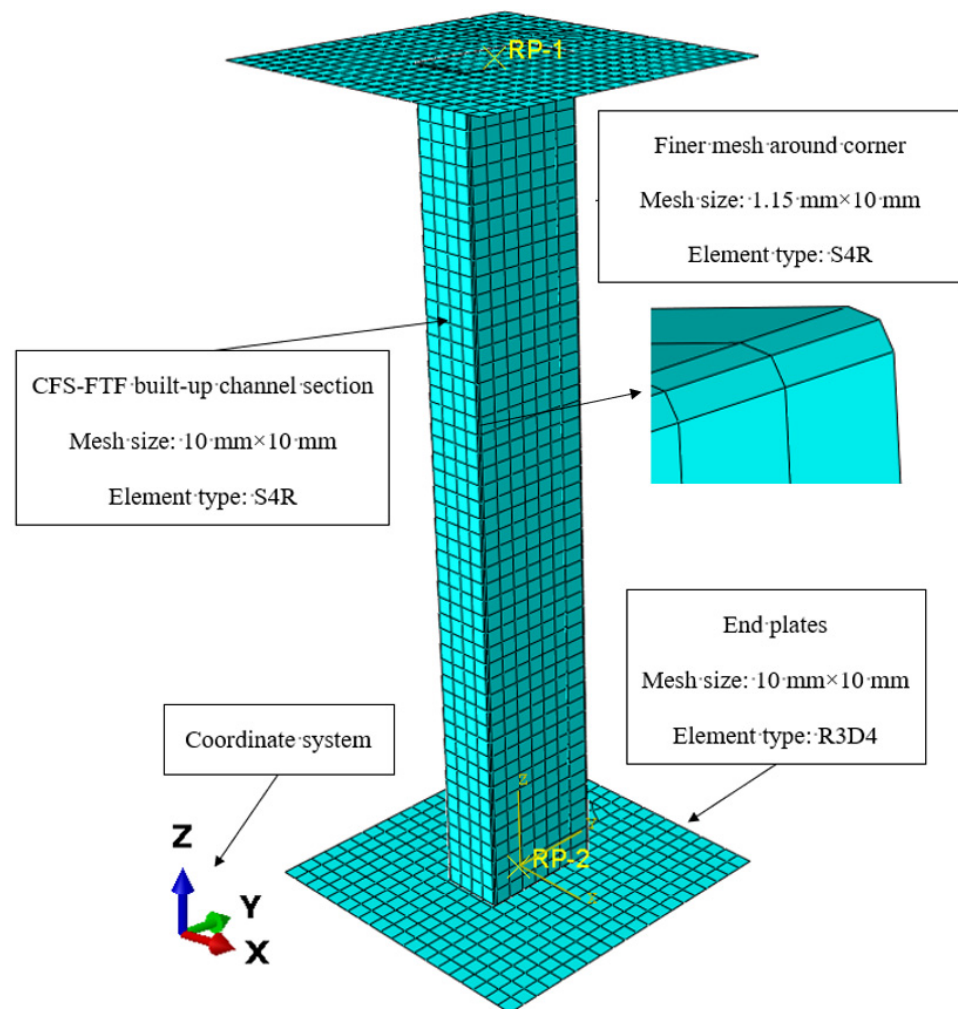


Figure 2. Meshing details used in FE models.

3.5. Boundary Conditions and Loadings

Figure 3 shows the detailed boundary and loading conditions of CFS-FTF built-up channel sections subjected to axial compression. The boundary condition of the pin-pin end support was simulated by loading displacements to both the top and bottom endplates at reference points. The translations in the X-axis and Y-axis were restrained to make sure that the top nodes could only move in the Z-axis. The rotation in the Y-axis was not restrained for the top nodes. For the bottom nodes of the endplate, the rotation in the Y-axis was released, while it was restrained for the other directions. In Figure 3, U1, U2, and U3 represent the displacements in the X-, Y-, and Z-axes, respectively. A 10 mm displacement was applied to all the FE models.

3.6. Contact Modelling

The “Surface-to-Surface” function was utilised to represent the relationship between the flanges and other overlapped surfaces in the CFS-FTF built-up sections. To ensure that no penetration occurred between the two surfaces, “Hard Contact” was set in the normal direction.

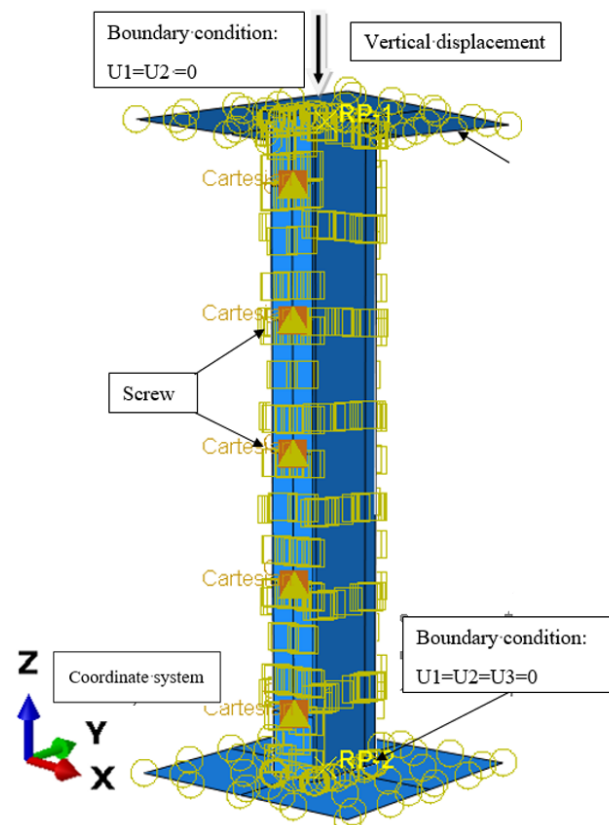


Figure 3. Boundary condition applied to the FE model of BL-L500-t1-S5.

3.7. Modelling of Imperfections

Imperfections were taken into consideration in the FEM. Local and overall imperfections were considered. The first eigenmode was used for each model after a buckling analysis was carried out to acquire the eigenmodes and eigenvalues for each CFS-FTF built-up channel section. The CFS-FTF built-up channel section imperfection magnitudes were scaled to the highest amplitude values in terms of the experiments [2]. Figure 4 displays the initial geometric imperfection eigenmodes of the local buckling and global buckling of BL-L500-t1-S5.

3.8. FE Validation

The comparison results of the axial capacities determined via the FEA with the experimental data in [2,18] are shown in Table 2. A sensitivity analysis of the initial imperfection was carried out on the specimen “BL75-L500-1” reported by Roy et al. [2]. For the FE model of this specimen, considering and neglecting the initial imperfections, the axial capacities of such a CFS-FTF built-up section are 132.0 kN and 132.6 kN, respectively. Hence, the initial imperfections were found to decrease the axial capacity of this specimen by around 0.5%. In comparison with the test data presented in [2], the average ratio of the axial capacities of P_{TEST}/P_{FEA} was 0.98 and the coefficient of variation (COVs) was 0.05 (see Table 2). Figure 5 displays the deformed shape of the section BL75-L500-t1-S5, as presented by the FEA, and the experimental failure mode was found to match reasonably well with the numerical one. The FE models show good accuracy in predicting the axial capacity of the CFS-FTF built-up channel sections reported in [2,18].

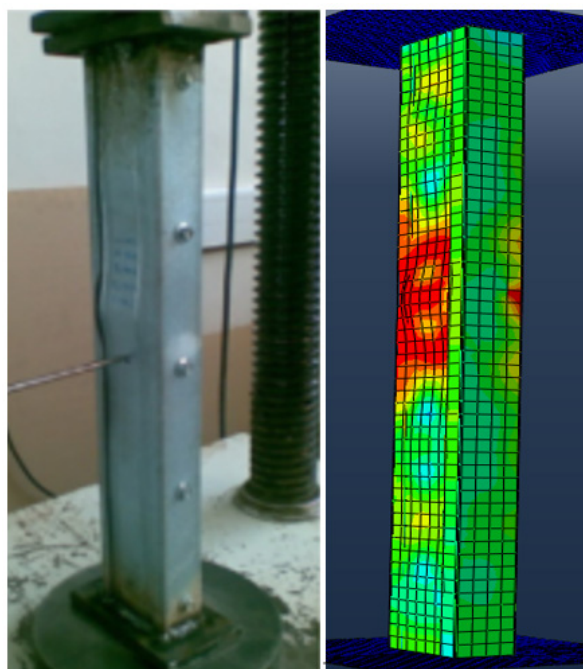


Figure 5. Deformed shapes at failure from the experiment [2] and FEA.

The validation in this section was conducted at ambient temperature. The modelling procedure of the CFS-FTF built-up columns at high temperature was kept the same as in the ambient temperature condition, although the material properties were changed to account for the lower yield stress and other material properties from the ambient to high temperatures.

4. Parametric Study

A parametric study was performed to study the influences of the thickness, member length, screw number, and high temperature on the structural performance of CFS-FTF built-up unlipped and lipped channels subjected to axial compression. The dimensions of the investigated sections are shown in Figure 1d,e.

4.1. Influence of the Thickness (t) on Axial Capacity (P)

Figure 6 depicts the influence of t on the axial capacity of the CFS-FTF built-up channel sections at high temperatures. For the FTF built-up unlipped channel columns made from G450 CFS, when t changes from 1.9 to 1.5 mm, the mean axial capacity changes from 148.6 kN to 93.2 kN (decrease of 37.3%) at high temperatures. Similarly, for the FTF built-up unlipped channel columns made from G250 CFS, when t changes from 1.95 to 1.55 mm, the mean axial capacity changes from 106.4 kN to 70.8 kN (decrease of 33.5%) at high temperatures.

For the FTF built-up lipped channel columns made from G450 CFS, when t changes from 1.9 to 1.5 mm, the mean axial capacity changes from 243.0 kN to 170.2 kN (decrease of 29.9%) at high temperatures. Similarly, for the FTF built-up lipped channel columns made from G250 CFS, when t changes from 1.95 to 1.55 mm, the mean axial capacity changes from 147.9 kN to 113.5 kN (decrease of 23.3%) at high temperatures.

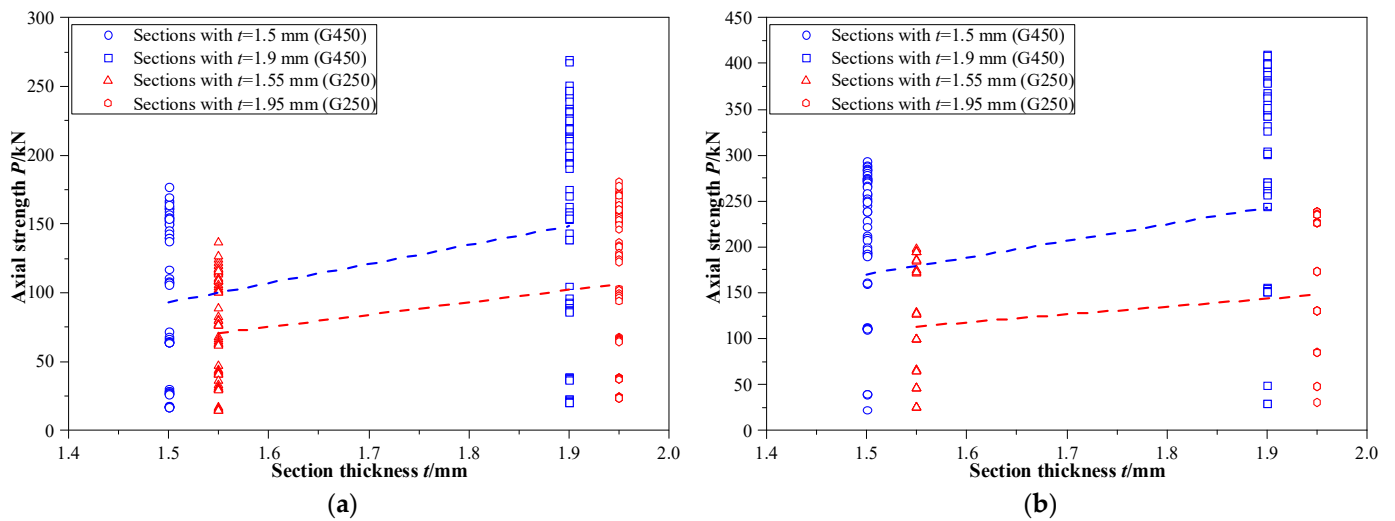


Figure 6. Influence of section thickness (t): (a) axial capacity of CFS-FTF built-up unlippped channel columns with different thicknesses; and (b) axial capacity of CFS-FTF built-up lippped channel columns with different thicknesses.

4.2. Influence of the Column Length (L) on Axial Capacity (P)

Figure 7 presents the influence of L on the axial capacity of the CFS-FTF built-up channel sections. For the FTF built-up unlippped channel sections, when L increases from 300 to 1500 mm, the mean axial capacity changes from 113.6 kN to 95.3 kN (decrease of 16.1%) at high temperatures. For the FTF built-up lippped channel columns, when L increases from 300 to 1500 mm, the mean axial capacity changes from 174.9 kN to 155.8 kN (decrease of 10.9%) at high temperatures.

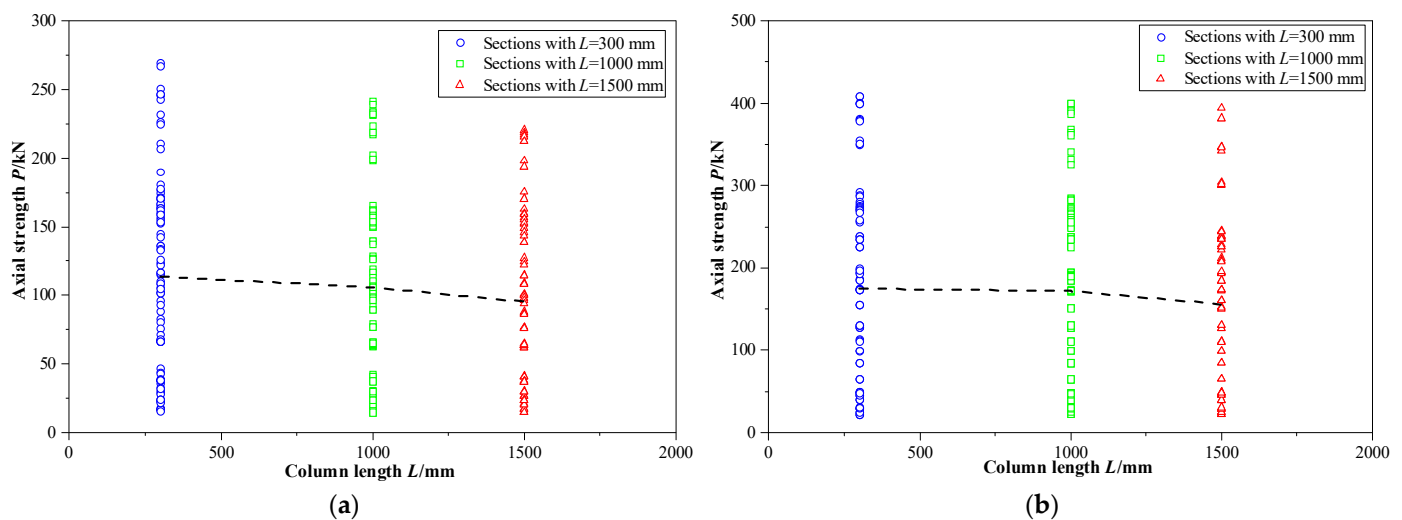


Figure 7. Influence of column length (L): (a) CFS-FTF built-up unlippped channel columns with different lengths; and (b) CFS-FTF built-up lippped channel columns with different lengths.

4.3. Influence of the Screws on Axial Capacity (P)

Figure 8 shows the influence of the screw number on the structural performance of the CFS-FTF built-up channel sections. For the FTF built-up unlippped channel columns, when the screw number (S) increases from two to five, the average axial capacity changes from 102.9 kN to 109.4 kN (increase of 6.3%) at high temperatures. For the FTF built-up lippped channel columns, when S increases from two to five, the average axial capacity changes from 170.1 kN to 192.8 kN (increase of 13.3%) at high temperatures.

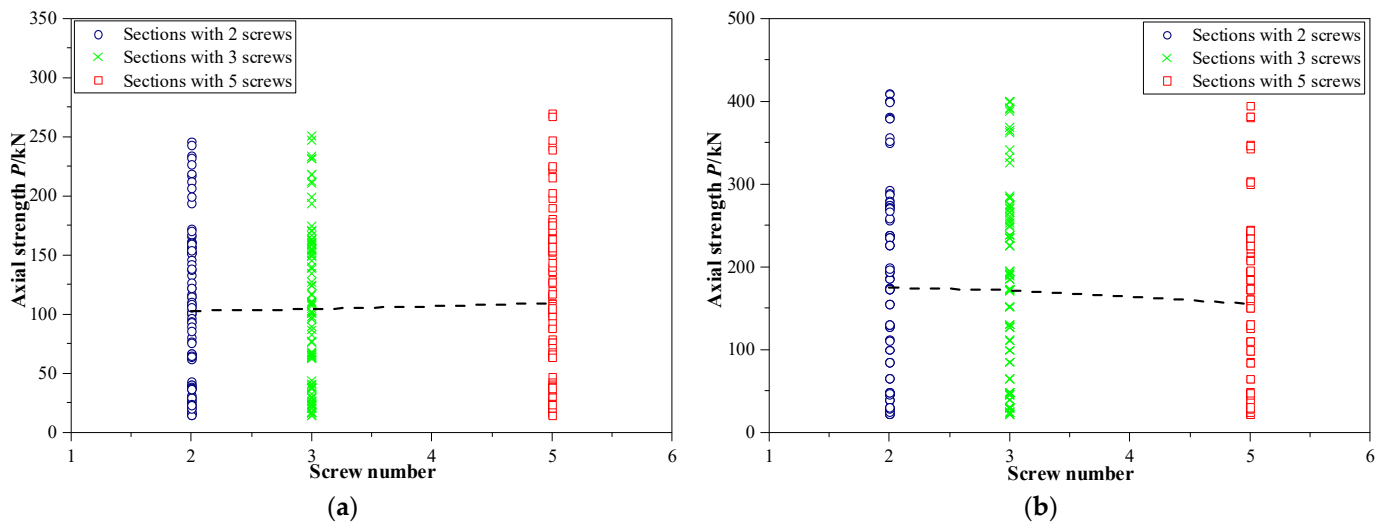


Figure 8. Influence of screw numbers (S): (a) CFS-FTF built-up unlippped channel columns with different screws; and (b) CFS-FTF built-up lippped channel columns with different screws.

The screws were evenly arranged along the column, and the distance from the side screw to the column end was 50 mm. Figure 9 shows the influence of the screw spacing on the structural performance of the CFS-FTF built-up channel sections. For the FTF built-up unlippped channel columns with a 300 mm length, the average axial capacity changes from 119.0 kN to 109.9 kN (decrease of 7.6%) at high temperatures when the screw spacing increases from 50 mm to 200 mm; while for the built-up lippped channel columns, the average axial capacity changes from 175.7 kN to 174.7 kN (decrease of 0.6%). For the FTF built-up unlippped channel columns with a 1000 mm length, the average axial capacity changes from 107.7 kN to 104.1 kN (decrease of 3.3%) at high temperatures when the screw spacing increases from 225 mm to 900 mm; while for the built-up lippped channel columns, the average axial capacity changes from 172.6 kN to 171.0 kN (decrease of 0.9%). For the FTF built-up unlippped channel columns with a 1500 mm length, the average axial capacity changes from 99.3 kN to 93.4 kN (decrease of 5.9%) at high temperatures when the screw spacing increases from 350 mm to 1400 mm; while for the built-up lippped channel columns, the average axial capacity changes from 157.4 kN to 156.6 kN (decrease of 0.5%). The effect of the screw distribution on the FTF built-up unlippped channel columns is more obvious than that on the lippped channel columns.

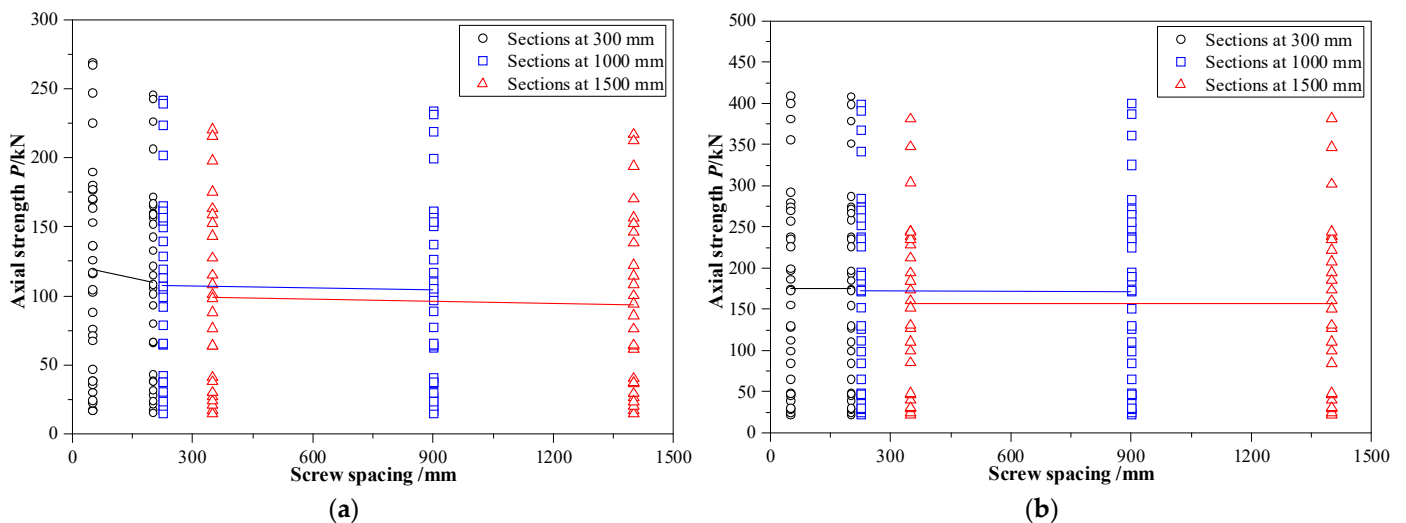


Figure 9. Influence of screw spacings: (a) CFS-FTF built-up unlippped channel columns with different screw spacings; and (b) CFS-FTF built-up lippped channel columns with different screw spacings.

4.4. Influence of the High Temperatures (T) on Axial Capacity (P)

Figure 10 shows the influence of T on the axial capacity of the CFS-FTF built-up channel sections. For the FTF built-up unlipped channel columns, as T increases from 20 to 700 °C, the mean axial capacity changes from 174.6 kN to 19.4 kN (decrease of 88.9%) at high temperatures. For the FTF built-up lipped channel columns, as T increases from 20 to 700 °C, the mean axial capacity changes from 270.2 kN to 26.6 kN (decrease of 90.2%) at high temperatures.

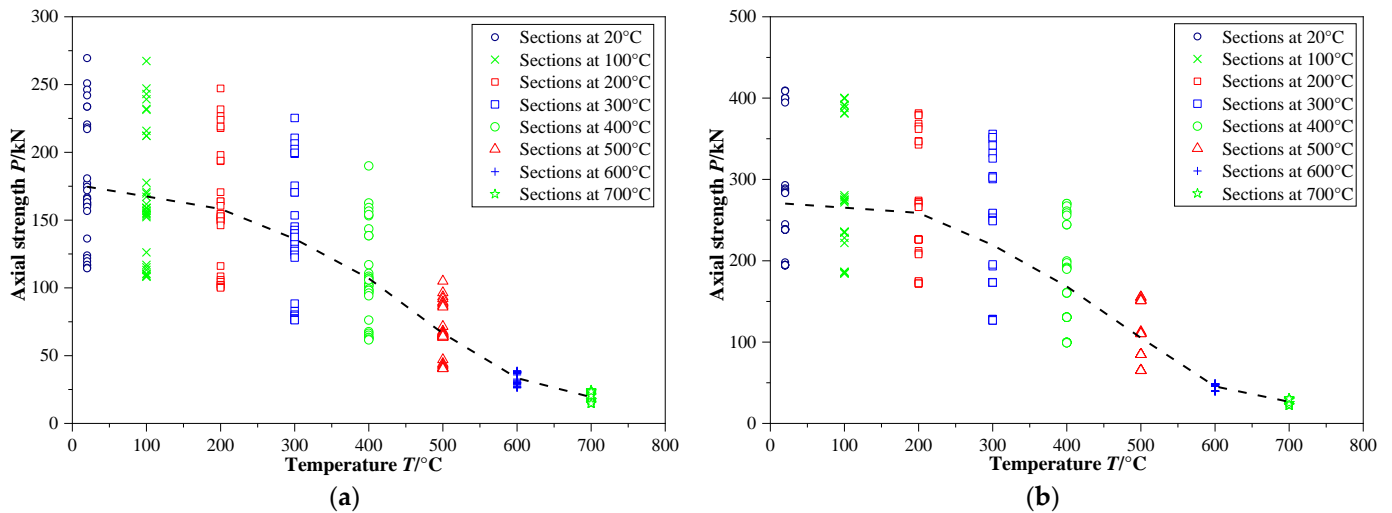


Figure 10. Influence of high temperatures (T): (a) CFS-FTF built-up unlipped channel columns at different temperatures; and (b) CFS-FTF built-up lipped channel columns at different temperatures.

4.5. Failure Modes

Figure 11 displays the failure modes of the CFS-FTF built-up channel sections. For the short and intermediate columns ($L = 300$ mm and 1000 mm, respectively), a coupled local and distortional buckling mode was the primary failure mode at room and high temperatures. For the slender columns ($L = 1500$ mm), a coupled distortional and flexural buckling mode was found to be the main failure mode.

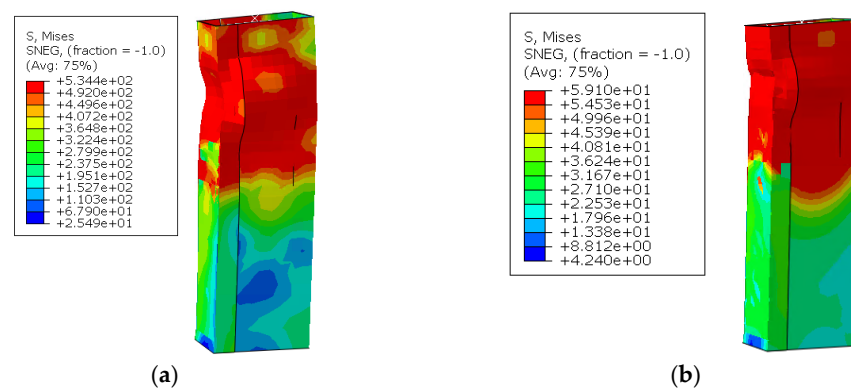


Figure 11. Cont.

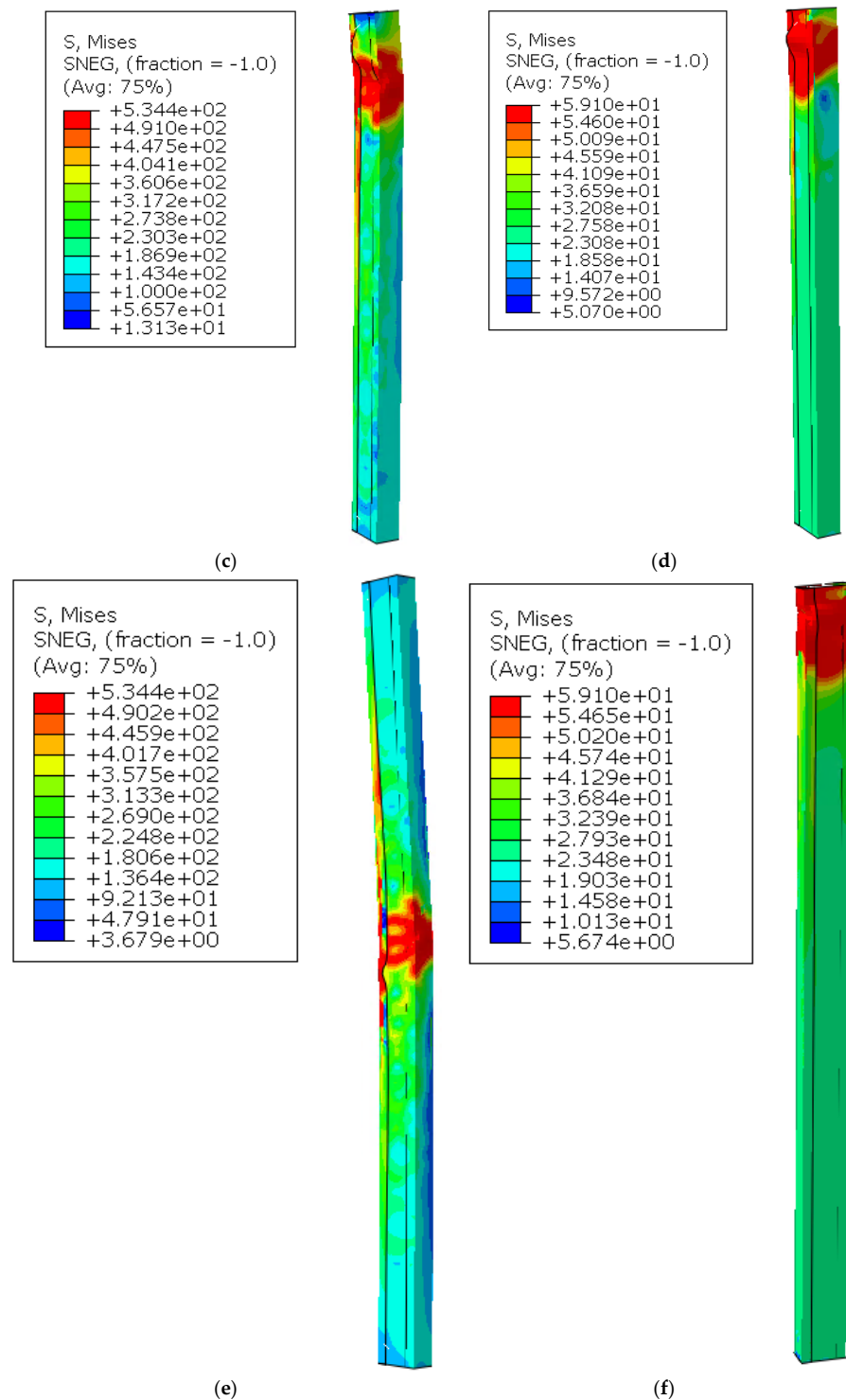


Figure 11. Buckling modes of CFS-FTF built-up columns: (a) BL-L300-t1.5-S5-T200; (b) BL-L300-t1.5-S5-T600; (c) BL-L1000-t1.5-S5-T200; (d) BL-L1000-t1.5-S5-T600; (e) BL-L1500-t1.5-S5-T200; and (f) BL-L1500-t1.5-S5-T600.

5. Design Guidelines

5.1. Effective Width Method (EWM) for CFS-FTF Built-Up Channel Sections

The axial capacities acquired from the experiments and FEA were compared with those calculated using the AISI (2016) [16] and AS/NZS (2018) [17]. The EWM in [16,17] was utilised to obtain the axial capacity of such sections. The design strengths of the CFS-FTF built-up columns were acquired in terms of the AISI (2016) [16] and AS/NZS

(2018) [17]. This can be referred to clause E2 of the AISI (2016) [16] and clause 3.4.1 of the AS/NZS (2018) [17].

$$P_{\text{AISI (2016) \& AS/NZS (2018)}} = A_e F_n \quad (1)$$

where A_e represents the cross-sectional area. The critical elastic buckling stress (F_n) was acquired in terms of Equations (2) and (3).

$$\text{For } \lambda_c \leq 1.5, F_n = (0.658 \lambda_c^2) f_y \quad (2)$$

$$\text{For } \lambda_c > 1.5, F_n = \left(\frac{0.877}{\lambda_c^2} \right) f_y \quad (3)$$

where f_y stands for the yield strength. The slenderness (λ_c) was obtained in terms of Equation (4).

$$\lambda_c = \sqrt{\frac{f_y}{f_{oc}}} \quad (4)$$

where f_y stands for the yield strength and f_{oc} stands for the buckling stress.

Equation (5) was utilised to consider the influence of the screws.

$$\left(\frac{KL}{r} \right)_m = \sqrt{\left(\frac{KL}{r} \right)_o^2 + \left(\frac{a}{r_i} \right)^2} \quad (5)$$

where $(KL/r)_m$ represents the modified global slenderness ratio, $(KL/r)_o$ represents the initial global slenderness ratio, K represents the boundary condition coefficient, a represents the screw spacing, and r_i represents the radius of gyration.

5.2. Comparison of FE Results with Design Strength

Figure 12 shows a comparison of the FE results with the design strengths calculated in terms of [16,17] for the CFS-FTF built-up columns. For the FTF built-up unlippped channel columns, the design strengths obtained from the EWM are conservative compared with the FEA axial capacities of different lengths. For the short columns (300 mm) of the FTF built-up lipped channel sections, the EWM is reasonably accurate in the prediction of the axial capacities at different high temperatures. Nonetheless, the design strengths obtained from the EWM are conservative compared with the FE results for the intermediate and slender columns (1000 mm and 1500 mm, respectively).

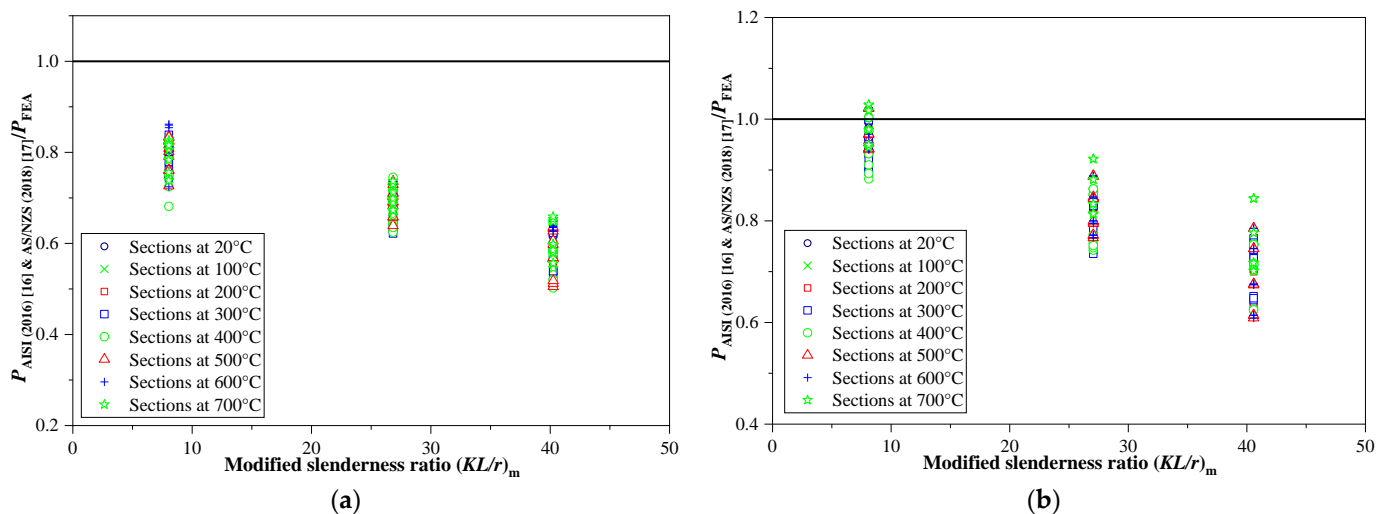


Figure 12. Comparison of FE strengths with design strengths: (a) $P_{\text{AS/NZS}}/P_{\text{FEA}}$ against modified slenderness for FTF built-up unlipped channel sections; and (b) $P_{\text{AS/NZS}}/P_{\text{FEA}}$ against modified slenderness for FTF built-up lipped channel sections.

6. Proposed Design Equations

6.1. New Equations

New design equations were proposed based on the FE results of the CFS-FTF built-up sections at high temperatures. The proposed equations comprise the relevant variables, including $(l_e/r)_m$ and f_{yT}/f_{y20} . A regression analysis was carried out, and different equations were proposed for the CFS-FTF unlippped and lippped channel sections as follows:

For the CFS-FTF built-up unlippped channel sections ($20\text{ }^\circ\text{C} \leq T \leq 700\text{ }^\circ\text{C}$):

$$R_{\text{prop}} = 0.015 \left(\frac{l_e}{r} \right)_m + 0.076 \frac{f_{yT}}{f_{y20}} + 1.08 \quad (6)$$

For the CFS-FTF built-up lippped channel sections ($20\text{ }^\circ\text{C} \leq T \leq 700\text{ }^\circ\text{C}$):

$$R_{\text{prop}} = 0.011 \left(\frac{l_e}{r} \right)_m + 0.106 \frac{f_{yT}}{f_{y20}} + 0.878 \quad (7)$$

where f_{y20} and f_{yT} represent the yield strength at room and high temperatures, and l_e represents the effective column length.

Figure 13 shows the ratios of the design strengths to the FE strengths of the CFS-FTF built-up channel sections at various high temperatures. In addition, a comparison of the prediction accuracy is presented. The mean ratio of the EWM strengths calculated using the AISI (2016) [16] and AS/NZS (2018) [17] to the FE strengths is 0.77, while the mean ratio of the proposed design strengths to the FE strengths is 1.01.

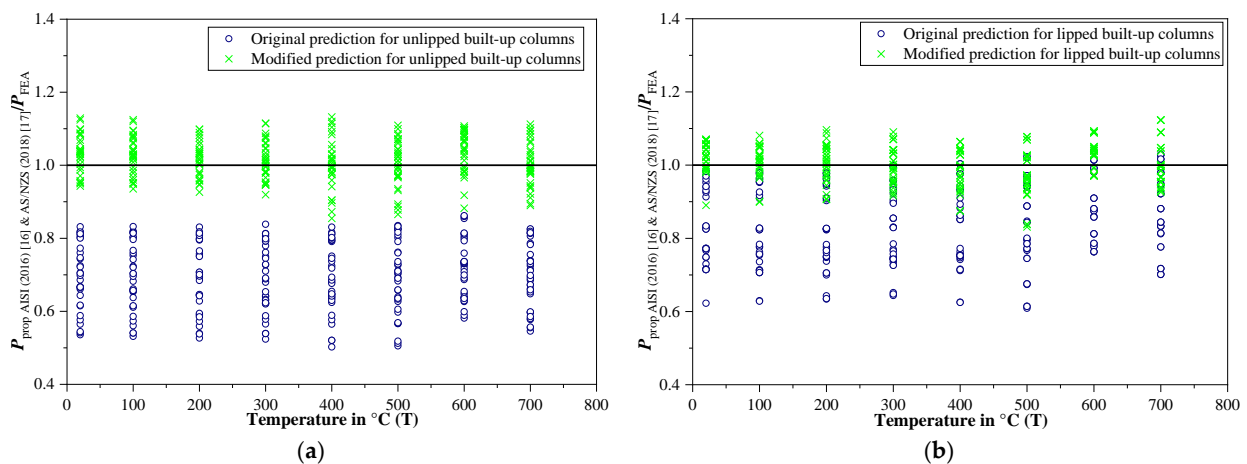


Figure 13. Comparison of FE strengths with proposed design strengths: (a) $P_{\text{AS/NZS}}/P_{\text{FEA}}$ of FTF built-up unlippped channel columns; and (b) $P_{\text{AS/NZS}}/P_{\text{FEA}}$ of FTF built-up lippped channel columns.

6.2. Reliability Analysis

The feasibility of the proposed design equations was evaluated via a reliability analysis. In terms of [16], when the reliability index of (β) is not less than 2.5, the equation is considered to be reliable, as per the guidelines of the AISI (2016) [16]. Equation (8) (as given below) [16] was used to calculate the reliability indices of the proposed design equations. In Equation (8), the values of M_m and V_m were taken as 1.1 and 0.1, respectively, which were determined based on the mean and COV values of the material factor. The values of F_m and V_f were 1.0 and 0.05, respectively, which were determined based on the mean and COV values of the fabrication factor. The value of V_q was set at 0.21, which again was determined based on the coefficient of variation (COV) value of the load factor. C_p represents the correction factor. The resistance factor ϕ was taken as 0.85 in terms of the AISI (2016) [16]. P_m represents the mean ratio of the proposed design strength to the FE strength.

$$\phi = CM_m F_m P_m \exp(-\beta \sqrt{V_m^2 + V_f^2 + C_p V_p^2 + V_q^2}) \quad (8)$$

Table 3 shows that the proposed reliability indexes are greater than 2.5 according to the AISI (2016) [16] for the CFS-FTF built-up channel sections at high temperatures. It also shows that the proposed equations are reliable in calculating the axial capacity of CFS-FTF built-up unlipped and lipped channel columns at high temperatures.

Table 3. Reliability analysis results.

	Proposed Equations	
	R_{prop} (Equation (6))/ R_{FEA}	R_{prop} (Equation (7))/ R_{FEA}
P_m	0.986	0.996
COV	0.058	0.054
φ [16]	0.85	0.85
β [16]	2.71	2.76

7. Conclusions

This study conducted a numerical study of the structural performance of CFS-FTF built-up channel columns at high temperatures subjected to axial compression. In total, 576 FE models were created, which were validated with the existing test data. A parametric investigation was performed to study the influences of the section thickness, member length, screw number and high temperature on the structural performance of these sections subjected to axial compression. Based on the numerical results, the following conclusions are reached.

The axial capacities of the investigated CFS-FTF built-up channel columns decreased as the temperature increased. As the temperature increased from 20 to 700 °C, a decline was observed in the axial capacity of the FTF built-up unlipped and lipped channels by 88.9% and 90.2% on average, respectively.

The EWM is conservative for the CFS-FTF built-up unlipped channel columns at various high temperatures. For the CFS-FTF built-up lipped channel columns, the EWM could provide close predictions for the strength of the columns with low modified slenderness. Nonetheless, the EWM cannot provide accurate predictions for the strengths of the intermediate and slender columns at room and high temperatures.

The local–distortional buckling mode was the main failure mode for the short and intermediate columns. For the slender columns, a coupled flexural buckling and distortional buckling mode were the main failure modes.

Based on the results of the numerical study, new equations were proposed to calculate the axial capacity of the CFS-FTF built-up channel sections at high temperatures. A reliability analysis was then performed, and the proposed equations were found to provide accurate predictions for the axial capacity of the CFS-FTF built-up channel sections at high temperatures.

Further research is required to include a heat transfer analysis in the FE modelling. The modelling procedure for CFS-FTF built-up channel columns at high temperatures is the same as that at ambient temperature, and only the material properties were changed to account for the lower yield stress and other material properties from the ambient to high temperatures. In addition, the simulation of fasteners at high temperatures should be taken into account in future studies.

Author Contributions: Conceptualization, Y.D., K.R. and Z.F.; methodology, Y.D., K.R. and Z.F.; software, Y.D.; validation, Y.D.; formal analysis, Y.D.; investigation, Y.D.; resources, Y.D. and K.R.; data curation, Y.D. and Z.F.; writing—original draft preparation, Y.D.; writing—review and editing, Y.D., K.R. and Z.F.; visualization, Y.D.; supervision, K.R., G.M.R. and J.B.P.L.; project administration, K.R., G.M.R. and J.B.P.L.; funding acquisition, K.R., G.M.R. and J.B.P.L. All authors have read and agreed to the published version of the manuscript.

Funding: This research received no external funding.

Data Availability Statement: Not applicable.

Conflicts of Interest: The authors declare no conflict of interest.

References

1. Roy, K.; Mohammadjani, C.; Lim, J.B.P. Experimental and numerical investigation into the behaviour of face-to-face built-up cold-formed steel channel sections under compression. *Thin-Walled Struct.* **2019**, *134*, 291–309. [[CrossRef](#)]
2. Roy, K.; Ting, T.C.H.; Lau, H.H.; Lim, J.B.P. Experimental and numerical investigations on the axial capacity of cold-formed steel built-up box sections. *J. Constr. Steel Res.* **2019**, *160*, 411–427. [[CrossRef](#)]
3. Gunalan, S.; Bandula, H.Y.; Mahendran, M. Local buckling studies of cold-formed steel compression members at elevated temperatures. *J. Constr. Steel Res.* **2015**, *108*, 31–45. [[CrossRef](#)]
4. Gunalan, S.; Bandula, H.Y.; Mahendran, M. Flexural–torsional buckling behavior and design of cold-formed steel compression members at elevated temperatures. *Eng. Struct.* **2014**, *79*, 149–168. [[CrossRef](#)]
5. Ranawaka, T.; Mahendran, M. Numerical modelling of light gauge cold-formed steel compression members subjected to distortional buckling at elevated temperatures. *Thin-Walled Struct.* **2010**, *48*, 334–344. [[CrossRef](#)]
6. Chen, J.; Young, B. Experimental investigation of cold-formed steel material at elevated temperatures. *Thin-Walled Struct.* **2007**, *45*, 96–110. [[CrossRef](#)]
7. Feng, M.; Wang, Y.C.; Davies, J.M. Structural behavior of cold-formed thin-walled short steel channel columns at elevated temperatures. Part 1: Experiments. *Thin-Walled Struct.* **2003**, *41*, 543–570. [[CrossRef](#)]
8. Landesmann, A.; Camotim, D. Distortional failure and DSM design of cold-formed steel lipped channel beams under elevated temperatures. *Thin-Walled Struct.* **2016**, *98*, 75–93. [[CrossRef](#)]
9. Laím, L.; Rodrigues, J.P.C.; Craveiro, H.D. Flexural behavior of axially and rotationally restrained cold-formed steel beams subjected to fire. *Thin-Walled Struct.* **2016**, *98*, 39–47. [[CrossRef](#)]
10. Dolamune Kankanamge, N.; Mahendran, M. Behavior and design of cold-formed steel beams subject to lateral–torsional buckling at elevated temperatures. *Thin-Walled Struct.* **2016**, *61*, 213–228. [[CrossRef](#)]
11. Fang, Z.; Roy, K.; Liang, H.; Poologanathan, K.; Ghosh, K.; Mohamed, A.M.; Lim, J.B.P. Numerical simulation and design recommendations for web crippling strength of cold-formed steel channels with web holes under interior-one-flange loading at elevated temperatures. *Build.* **2021**, *11*, 666. [[CrossRef](#)]
12. Fang, Z.; Roy, K.; Lakshmanan, D.; Pranomrum, P.; Li, F.; Lau, H.H.; Lim, J.B.P. Structural behaviour of back-to-back cold-formed steel channel sections with web openings under axial compression at elevated temperatures. *J. Build. Eng.* **2022**, *54*, 104512. [[CrossRef](#)]
13. Yang, J.; Wang, W.; Shi, Y.; Xu, L. Experimental study on fire resistance of cold-formed steel built-up box columns. *Thin-Walled Struct.* **2020**, *147*, 106564. [[CrossRef](#)]
14. Yang, J.; Shi, Y.; Wang, W.; Xu, L.; Al-azzani, H. Experimental and numerical studies on axially restrained cold-formed steel built-up box columns at elevated temperatures. *J. Constr. Steel Res.* **2020**, *171*, 106143. [[CrossRef](#)]
15. Pires, T.A.C.; Silva, J.J.D.R.; Santos, M.M.L.D.; Costa, L.M. Fire resistance of built-up cold-formed steel columns. *J. Constr. Steel Res.* **2021**, *177*, 106456. [[CrossRef](#)]
16. American Iron and Steel Institute, AISI. *North American Specification for the Design of Cold-Formed Steel Structural Members*; American Iron and Steel Institute: Washington, DC, USA, 2016.
17. AS/NZS 4600:2018; Australia/New Zealand Standard (AS/NZS), Cold-Formed Steel Structures. Standards Australia; Standards New Zealand: Sydney, Australia; Wellington, New Zealand, 2018.
18. Selvaraj, S.; Madhavan, M. Design of cold-formed steel built-up closed section columns using direct strength method. *Thin-Walled Struct.* **2022**, *171*, 108746. [[CrossRef](#)]
19. *ABAQUS Analysis User's Manual*; Version 6.14-2; ABAQUS Inc.: Palo Alto, CA, USA, 2018.
20. Kankanamge, N.D.; Mahendran, M. Mechanical properties of cold formed steel at elevated temperatures. *Thin-Walled Struct.* **2011**, *49*, 26–44. [[CrossRef](#)]
21. Dai, Y.; Roy, K.; Fang, Z.; Chen, B.; Raftery, G.M.; Lim, J.B.P. A novel machine learning model to predict the moment capacity of cold-formed steel channel beams with edge-stiffened and un-stiffened web holes. *J. Build. Eng.* **2022**, *53*, 104592. [[CrossRef](#)]
22. Fang, Z.; Roy, K.; Xu, J.; Dai, Y.; Paul, B.; Lim, J.B.P. A novel machine learning method to investigate the web crippling behaviour of perforated roll-formed aluminium alloy unlippped channels under interior-two flange loading. *J. Build. Eng.* **2022**, *51*, 104261. [[CrossRef](#)]
23. Fang, Z.; Roy, K.; Dai, Y.; Lim, J.B.P. Effect of web perforations on end-two-flange web crippling behaviour of roll-formed aluminium alloy unlippped channels through experimental test, numerical simulation and deep learning. *Thin-Walled Struct.* **2022**, *179*, 109489. [[CrossRef](#)]

Disclaimer/Publisher's Note: The statements, opinions and data contained in all publications are solely those of the individual author(s) and contributor(s) and not of MDPI and/or the editor(s). MDPI and/or the editor(s) disclaim responsibility for any injury to people or property resulting from any ideas, methods, instructions or products referred to in the content.